Chlorophyll Fluorescence Imaging of Leaves and Fruits

Article · January 2004

DOI: 10.1007/978-1-4020-3218-9_14

2 authors:

Ladislav Nedbal
Forschungszentrum Jülich

John Whitmarsh
Association for Frontotemporal Degeneration

Chapter 14

Chlorophyll Fluorescence Imaging of Leaves and Fruits[1]

Ladislav Nedbal*
Laboratory of Applied Photobiology and Bio-Imaging, Institute of Landscape Ecology, Academy of Sciences of the Czech Republic, and Institute of Physical Biology, University of S. Bohemia, Zámek 136, CZ-37333 Nové Hrady, Czech Republic

John Whitmarsh†
Department of Biochemistry, University of Illinois and Photosynthesis Research Unit, USDA/ARS, Urbana, IL 61801, U.S.A.

Note: The disk contained color files, but no camera-ready hard copies were included in the packet. Please send high quality glossy color figures.

[1] This chapter is dedicated to Dr. Ivan Šetlik in honor of his many years of research and service to the photosynthesis community. *Author for correspondence, email: nedbal@greentech.cz. † Present address: National Institute of General Medical Sciences, National Institutes of Health, 45 Center Drive, Bethesda, MD 20892-6200, U.S.A.

George C. Papageorgiou and Govindjee (eds): Chlorophyll Fluorescence: A Signature of Photosynthesis, pp. 000–000.

Summary

Chlorophyll fluorescence imaging provides a powerful, non-invasive tool for investigating leaf photosynthesis under natural conditions. Applications of fluorescence imaging in plant research are increasing rapidly, ranging from basic discoveries to biotechnology. Fluorescence imaging reveals a wide range of internal leaf characteristics, including spatial variations due to differences in physiology, development, nutritional state, pigment distribution, and morphology, and optical properties. Using distinct chlorophyll fluorescence signatures, imaging technology is being used for high throughput mutant screening, as well as early detection of biotic and abiotic stresses. In this chapter we describe the technology and methodology used to image chlorophyll fluorescence and discuss applications that illustrate advantages offered by imaging analysis.

I. Introduction

A. Why Image?

More than seventy years ago Kautsky and Hirsch (1931) moved a plant from darkness into blue light and viewed it through a red filter that allowed them to observe chlorophyll (Chl) fluorescence with their eyes. At first the plant gave off a dull red glow, but as they watched, the usual static view of a plant was replaced by a dynamic image as the red glow increased rapidly to a brighter red and then slowly decreased (see http://www.life.uiuc.edu/govindjee/movkautsky.html and http://www.greentech.cz/lapi/about/kautsky/index.html). This observation likely marks the first kinetic imaging of Chl fluorescence from leaves. Beginning with these early experiments, measurements of Chl fluorescence emission have been highly successful in enhancing our understanding of photosynthesis, and over the past three decades have emerged as one of the most widely used tools for monitoring photosynthetic performance in vivo. This success is built on a deep understanding of the intimate relationship between Chl fluorescence dynamics and the inner workings of the photosynthetic light reactions and photosynthetic carbon reduction cycle. Today, the range of photosynthetic processes and plant responses that can be monitored by Chl fluorescence measurements include the quantum efficiency of Photosystem II (PS II), the redox state of the primary quinone acceptor (Q_A) of PS II, the redox state of the plastoquinone pool, the transitions between the S-states of the oxygen evolving complex, the rate of steady state linear electron transport, Photosystem I (PS I) cyclic electron transport, biotic and abiotic stresses, and much more[2].

Although efforts to image Chl fluorescence have been going on for decades, it is due to advancements in the technology of light emission, imaging detectors, and rapid data handling that have allowed modern instrumentation to be developed that is effective, simple to use, and affordable. Most modern imaging instruments can trace their lineage back to the innovative work of Omasa et al. (1987) who introduced a detector array that captured a two-dimensional image of thousands of fluorescence transients from a leaf. The technique allows captured fluorescence transients to be analyzed individually, or integrated in image segments that correspond to individual plants, single leaves, selected leaf areas, or cells, yielding detailed information about spatial and kinetic heterogeneity of plant activity. The capacity to resolve photosynthetic performance over the surface of a leaf distinguishes Chl fluorescence imaging from integrative methods such as gas exchange or non-imaging Chl fluorometry[3].

Not surprisingly, the molecular and physiological processes that alter the yield of Chl fluorescence can

Abbreviations: CCD – charge coupled device; Chl – chlorophyll; DCMU – 3-(3′,4′-dichlorophenyl)-1,1-dimethylurea; F_0 – fluorescence emission measured when the primary quinone acceptor Q_A is oxidized and non-photochemical quenching is inactive; F_0' – fluorescence emission measured when Q_A is oxidized and non-photochemical quenching is active; F_M – maximum fluorescence emission measured when Q_A and the plastoquinone pool are reduced and non-photochemical quenching is inactive ; F_M' – fluorescence emission measured when Q_A and plastoquinone pool are reduced and non-photochemical quenching is active; F_S – steady-state fluorescence emission in light; F_V – variable fluorescence measured in the absence of non-photochemical quenching ($F_V = F_M - F_0$); F_V' – variable fluorescence measured when non-photochemical quenching is active ($F_V' = F_M' - F_0'$); NPQ – non-photochemical quenching of the excited state of chlorophyll; PS II – Photosystem II; Q_A – primary quinone acceptor of Photosystem II; Q_B – secondary quinone acceptor of Photosystem II

[2] For relation of Chl fluorescence to PS II reactions, see Shinkarev, this volume. [3] References to all the early fluorescence imaging measurements are available in Govindjee and Nedbal (2000).

vary over the surface of a leaf, giving rise to spatial heterogeneity that can be detected by imaging. Fluorescence heterogeneity can be caused by external factors, such as abiotic stress, or by internal factors, such as variations in leaf physiology during development. Under such conditions, Chl fluorescence imaging provides a non-invasive tool to reveal and understand spatial heterogeneity in leaf performance.

The application of fluorescence imaging in plant research is growing rapidly, ranging from basic research to high throughput screening in biotechnology. Fluorescence imaging is currently employed to visualize photosynthetic heterogeneity caused by localized biotic stress (Balachandran et al., 1994; Esfeld et al., 1995; Ning et al., 1995; Peterson and Aylor, 1995; Scholes and Rolfe, 1996; Bowyer et al., 1998; Osmond et al., 1998; Lohaus et al., 2000; Nedbal et al., 2000b). Fluorescence imaging is also used to reveal local effects of abiotic stress, such as the effect of high or low temperatures or drought on plant performance (Gibbons and Smille, 1980; Omasa et al., 1987; Daley et al., 1989; Ning et al., 1995; Meyer and Genty, 1999; Osmond et al., 1999b; Barták et al., 2000; Lichtenthaler and Babani, 2000, also elsewhere in this volume). Because fluorescence emission is extremely sensitive to non-uniform incident light (Ning et al., 1997; Osmond et al., 1999a; Oxborough, this volume), fluorescence imaging can be used to investigate effects of shading in a canopy. The power of fluorescence imaging derives from its ability to reveal a wide range of internal plant characteristics that induce emission heterogeneity, including spatial variations due to differences in physiology, the developmental stage (Mott et al., 1993; Cardon et al., 1994; Genty and Meyer, 1994; Siebke and Weis, 1995a,b; Bro et al., 1996; Eckstein et al., 1996; Meyer and Genty, 1998; Lichtenthaler and Babani, 2000), the nutritional state (Heisel et al., 1996; Langsdorf et al., 2000), pigment distribution, and morphology and optical properties (Hoque and Remus, 1994; Takahashi et al., 1994; Lichtenthaler et al., 1996; Koizumi et al., 1998). A distinct Chl fluorescence signature provides a rapid means to screen for mutant colonies or mutant plants (Gibbons and Smille, 1980; Fenton and Crofts, 1990; Bennoun and Béal, 1997; Niyogi et al., 1997; Niyogi et al., 1998; Shikanai et al., 1998; Peterson and Havir, 2000; Varotto et al., 2000). As illustrated by these few examples, Chl fluorescence imaging provides a powerful tool for investigating leaf photosynthesis under natural conditions. In addition, the fact that Chl fluorescence can be imaged from the molecular level to grasslands, crops, and forests, opens the way to scale photosynthetic performance from the membrane, to the chloroplast, to the leaf, and eventually to the field.

The aim of this chapter is to describe the technology and methodology used to image Chl fluorescence of leaves. Because imaging instruments are equally successful at imaging photosynthetic bacteria, algae, and whole plants, much of the information contained here applies to these systems as well. Interpreting fluorescence imaging data requires an understanding of how chlorophyll fluorescence measurements are analyzed and interpreted. Descriptions of the fundamentals of Chl fluorescence can be found in various chapters in Govindjee et al., 1986 and elsewhere (Dau, 1994; Falkowski and Kolber, 1995; Govindjee, 1995; Kramer and Crofts, 1996; Strasser et al., 1998; Lazár, 1999; Krause and Jahns, 2002; Nedbal and Koblížek, 2003). Below we first describe imaging instrumentation and technology, and then discuss selected applications that illustrate advantages offered by imaging analysis. Although the examples discussed are few, we have included a large number of references to work that includes data from Chl fluorescence imaging. Fortunately, the field is young and the literature is not yet overwhelming. Because imaging instrumentation and software are rapidly improving, we discuss the technological and biological factors that currently limit the usefulness of the technique. However, it is fair to say that Chl imaging has come of age, and imaging instrumentation can now provide two dimensional maps of Chl fluorescence parameters that are comparable to what was done in the past using non-imaging Chl fluorometers.

B. A. Case Study

Instruments for imaging Chl fluorescence over a leaf are designed to measure a range of fluorescence parameters[4]. Optimally, an instrument designed to image Chl fluorescence should provide a map of five key fluorescence parameters: F_0, F_0', F_M, F_M', and F_S (see Abbreviations for definitions). Similar to non-imaging pulse amplitude modulation (PAM) fluorometers, an imaging fluorometer can be designed to control the opening time of the detector, so that it is

[4] Commercial instruments for imaging Chl fluorescence are currently available from P.S.I., (www.psi.cz); Qubit, (www.qubitsystems.com); and Walz, (www.walz.com).

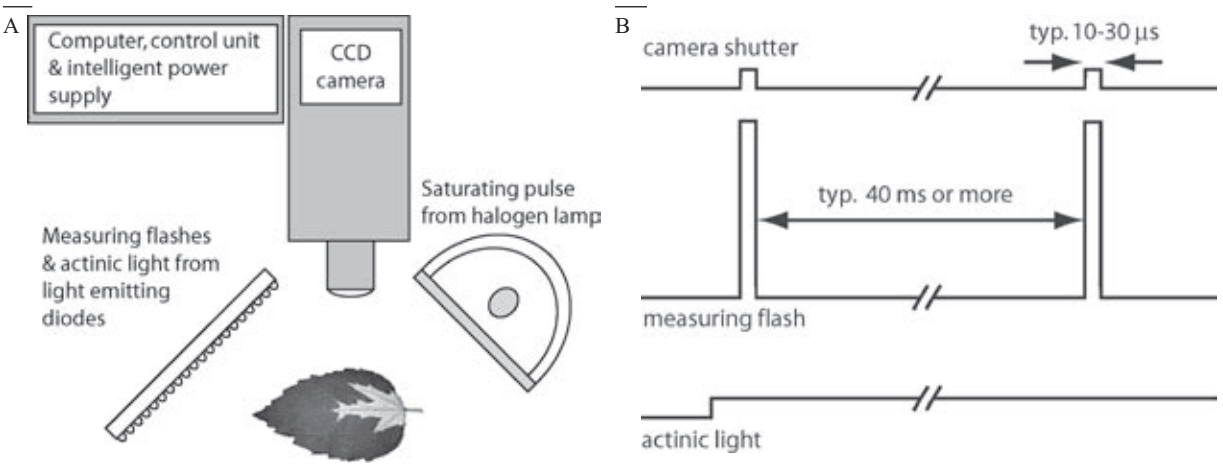

Fig. 1. A. Schematic of a chlorophyll imaging instrument showing key elements. The charge coupled device (CCD) camera has a filter that passes red and far-red light ($\lambda > 690$ nm). The camera images fluorescence from a leaf that is exposed to measuring light flashes generated by an array of orange ($\lambda_{max} \approx 635$ nm) light emitting diodes (LEDs). The LEDs also provide continuous actinic light. Brief intense light pulses (typically 1 s) for measuring F_M and F_M' (saturating for plastoquinone reduction) are generated by a 250 W halogen lamp equipped with a dichroic mirror that blocks light above 650 nm. Software allows the user to design experimental protocols (e.g., illumination regimes). The experimental protocol is executed by the control unit and an intelligent power supply. Software is designed so that the user determines the image segments for kinetic analysis (e.g., selected leaf areas, algal colonies, individual plants), data *presentation and visualization (e.g., images of F_0, F_v'/F_M'). B.* Timing diagram showing the synchronous operation of the electronic shutter of the CCD camera (top line) with the measuring flashes (middle line). The actinic light is shown schematically in the bottom line.

synchronous with the extremely short measuring light pulses (Fig.1). The resolving power of a fluorescence imaging instrument is readily shown by monitoring inhibition of photosynthesis as a herbicide infiltrates a leaf (Daley et al., 1989; Fenton and Crofts, 1990; Yanase and Andoh, 1992; Ning et al., 1995; Rolfe and Scholes, 1995; Lichtenthaler et al., 1997; Nedbal et al., 2000a). Figure 2 shows an example in which an African violet leaf (*Saintpaulia*) was detached and its petiole placed in a solution containing DCMU (3-(3′,4′-dichlorophenyl)-1,1-dimethylurea), a Photosystem II (PS II) inhibitor. As the inhibitor infiltrates the leaf along its major veins, the fluorescence yield F_S of the inhibited area increases because the DCMU blocks electron flow through PS II by binding to the Q_B site (Velthuys, 1981). A secondary effect of the herbicide is to lower non-photochemical fluorescence quenching by blocking the energization of the thylakoid membrane. In this experiment, Chl fluorescence was excited using modulated light provided by an array of orange light emitting diodes (LEDs) as shown in Fig. 1. Actinic light was generated by the same light source. A 250 W tungsten-halogen lamp provided saturating light pulses. Chl fluorescence was detected by a charge coupled device (CCD) camera that captured the fluorescence kinetics of a leaf in a 2-dimensional array of 120,000 detector elements (for experimental details, see Nedbal et al., 2000a). Figure 2B shows the relative Chl fluorescence yield for the area of the leaf infiltrated with DCMU (diamonds) and for the leaf area outside the infiltrated region (open circles). The fluorescence was calculated by averaging all the data points within the selected areas. For purposes of comparison, the data for the entire leaf was also averaged (solid circles). Note that integration over the entire surface of the leaf, which is equivalent to a non-imaging fluorescence measurement[5], did not reveal any significant inhibition. This example demonstrates the limitation of non-imaging instrumentation to reveal inhibition in the case of a significant functional heterogeneity.

Interpretation and analysis of Chl fluorescence images is made possible by decades of work based on non-imaging chlorophyll fluorescence measure-

[5] Non-imaging fluorometry effectively averages the fluorescence signal over the area of the leaf illuminated by the measuring light (e.g., a light guide). This is equivalent to integrating a corresponding area of the leaf in imaging fluorometry ($F^{non\text{-}imaging} \approx \Sigma F_{pixel}$). An important limitation of non-imaging fluorometry is the fact that the ratio $[(F_M - F_0)/F_M]^{non\text{-}imaging} = (\Sigma F_{M,pixel} - \Sigma F_{0,pixel})/\Sigma F_{M,pixel}$ obtained by a non-imaging instrument, and the ratio $[(F_M - F_0)/F_M]^{imaging} = \Sigma [(F_{M,pixel} - F_{0,pixel})/F_{M,pixel}]$ obtained by an imaging instrument, are not identical unless the signal is homogenous over the selected leaf area (Genty and Meyer, 1994; Siebke and Weiss, 1995a; Oxborough and Baker, 1997b).

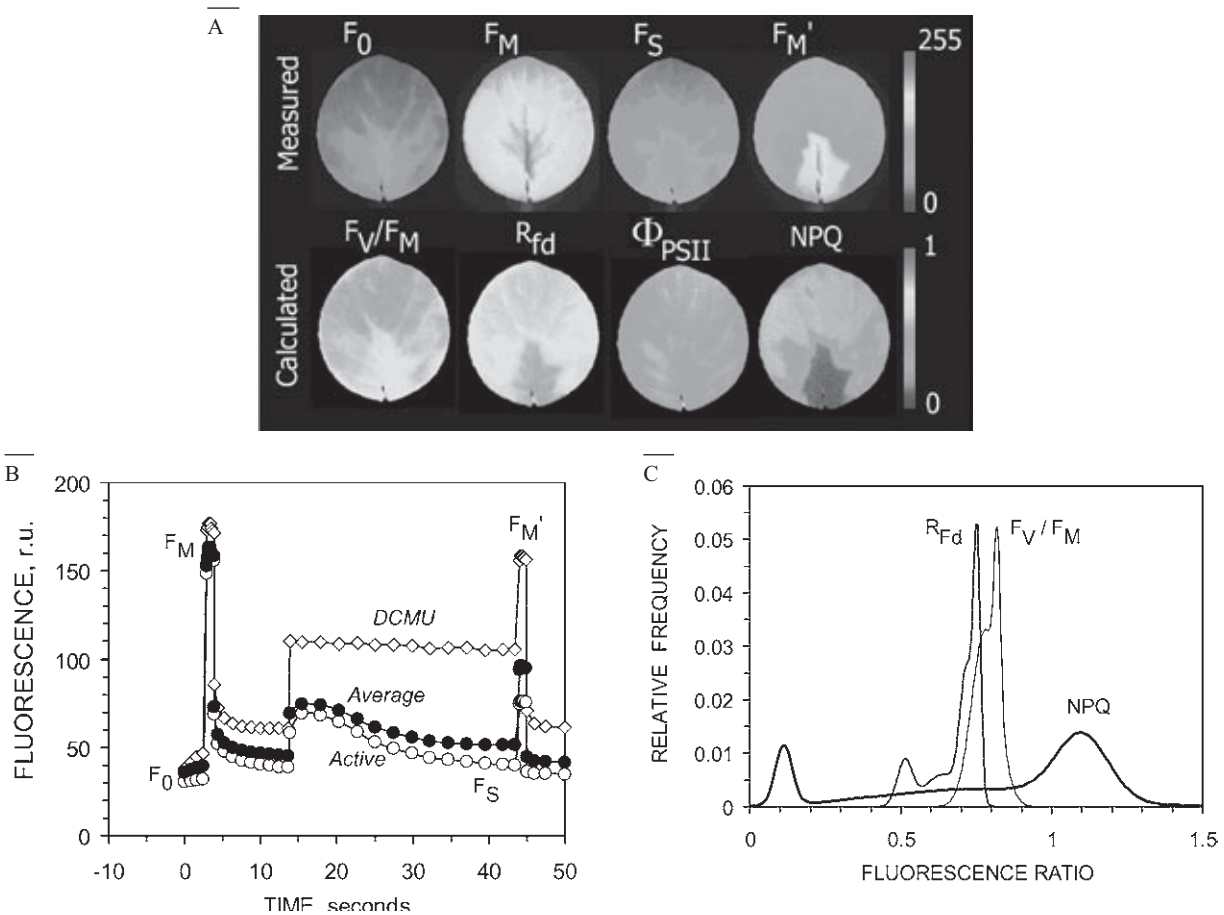

Fig. 2. (A) Images of chlorophyll fluorescence showing F_0, F_M, F_S, and F_M' for an African violet leaf (*Saintpaulia*) infiltrated by the Photosystem II inhibitor DCMU (top row). The bottom row shows the ratios F_V/F_M (= $(F_M - F_0)/F_M$,), R_{fd} (= $(F_M - F_S)/F_M$), $\Phi_{PS\,II}$ (= $(F_M' - F_S)/F_M'$), and NPQ (= $(F_M - F_M')/F_M'$) calculated pixel-by-pixel using the data in the top row. The numerical values shown to the left of the rows are color-coded using a red (high level) to blue (low level) color scale (for color images see the color section of this volume). Further details are given in the text and in Nedbal et al. (2000). (B) Kinetics of the chlorophyll fluorescence emission from an African violet leaf partially infiltrated by DCMU (see abbreviations list) calculated from the images shown in Fig. 2A. The numerical values in Fig. 2B were obtained by integration over: the area infiltrated by DCMU (◇), the area not affected by DCMU (*Active*, ○); and the entire surface of the leaf (*Average*, ●). The fluorescence was measured first for the dark-adapted leaf (F_0). Then the leaf was illuminated by a 1 second pulse of high intensity light (3000 μmol(photons) m^{-2} s^{-1}) for determination of the maximum fluorescence F_M. After a dark relaxation period, the leaf was illuminated by continuous actinic light (300 μmol(photons) m^{-2} s^{-1}) starting at t = 13 s. The steady state fluorescence F_S was measured at t = 43 s, then a second pulse of saturating light was given to determine the maximum fluorescence of the light-adapted leaf (F_M'). A detailed description of the experimental protocol is given in Nedbal et al. (2000). C. Histograms calculated from the images of F_V/F_M, R_{Fd}, and non-photochemical quenching NPQ (see abbreviations list). Histograms show the relative frequency of pixels versus the calculated value of the respective fluorescence ratio. Further details are given in the text. The DCMU infiltrated areas were defined by pixels with a NPQ below 0.2, whereas the active areas were defined by pixels with NPQ greater than 0.9.

ments (reviewed lately by Dau, 1994; Falkowski and Kolber, 1995; Govindjee, 1995; Kramer and Crofts, 1996; Strasser et al., 1998; Lazár, 1999; Krause and Jahns, 2002; Nedbal and Koblížek, 2003 and other chapters in this volume). The early studies revealed the mechanistic relationship between chlorophyll fluorescence and photosynthesis and established useful relationships for estimating rates and efficiencies. One of the most frequently used relationships is the ratio $F_V/F_M = (F_M - F_0)/F_M$, which is proportional to the maximum quantum yield of Photosystem II photochemistry (Krause et al., Schreiber et al., Strasser et al., this volume). An image of F_V/F_M (bottom row) calculated for each pixel using the F_M and F_0

images is shown in the top row of the figure. Other relationships commonly used in assessing photosynthetic performance by kinetic imaging include the fluorescence decrease ratio [$R_{Fd} = (F_M - F_S)/F_M$] (Ning et al., 1995; Lichtenthaler and Miehé, 1997; see Lichthenthaler and Babani, this volume), the apparent quantum efficiency of PS II in a light exposed leaf $\phi_{PS\,II} = (F'_M - F_S)/ F'_M$] (Genty and Meyer, 1994), and the Stern-Volmer non-photochemical quenching ratio NPQ = $(F_M - F'_M)/F'_M$ (Bilger and Björkman, 1990; Gilmore and Niyogi et al., this volume). The choice of the fluorescence parameter or relationship to focus on depends on the physiological and experimental conditions. In some cases, histograms that plot the numbers of pixels with fluorescence value in a selected range are an effective way to reveal significant heterogeneity. Fig. 2C shows histograms of the fluorescence ratios: NPQ (see above), F_V/F_M, and R_{Fd}. Note that for F_V/F_M nearly all pixels are in the range of 0.820 ± 0.015. In contrast, the histograms of NPQ and of R_{Fd} exhibit a notable heterogeneity, providing a clear distinction between active and inhibited areas of the leaf.

II. Imaging Technology and Techniques

Imaging Chl fluorescence depends on four basic processes: (1) image capture: illumination, data capture, digitalization, and data transfer to a computer, (2) image segmentation: use of selection tools to define relevant areas or structures for analysis, (3) analysis: calculation of fluorescence parameters and kinetics for each of the image segments, and (4) data visualization. The basic imaging hardware consists of light sources, an imaging detector, a control unit, a power supply, and a computer (Fig.1). The components that determine image quality and system cost are the light sources and the detectors (discussed in Sections II.A. and II.B.). The software that drives the instrumentation and analysis, and serves as the interface between the user and the instrument, is a critical factor in determining the usefulness of an imaging fluorometer. The software must provide data handling routines that allow the user to readily visualize images and to divide images into selected areas based on calculated fluorescence parameters. These operations require calculations of parameters over selected regions that depend on pixel-by-pixel arithmetic operations (discussed in Section II.C). In addition, the software must enable the user to design sophisticated experimental protocols that control light sources and image capture sequences (discussed in Section II.D). Some of the important factors that currently limit imaging fluorometers are discussed in Section II.E. In general it can be said that the quality of imaging instruments used in plant research is limited by cost versus performance considerations (high-end imaging instruments are extremely expensive). Finally, we discuss problems imposed by the use of two-dimensional fluorescence images in leaves where the fluorescence signals are significantly influenced by absorption, re-absorption of fluorescence, and scattering (Section II.F).

A. Light Sources

1. Continuous Light Sources

Early imaging instruments used a single, high-intensity continuous light source that served to drive photochemistry and to excite the fluorescence emission captured by the imaging detector (Omasa et al., 1987; Daley et al., 1989; Ning et al., 1995; Siebke and Weis, 1995a). This design offers the advantage of a relatively intense fluorescence signal, which improves the signal to noise ratio, but creates fluorescence transients that are too fast to be captured by a CCD camera. A typical CCD camera captures about 25 images/second. The problem is that during the long integration period (typically 20 ms), PS II turns over several times in high light, which increases the fluorescence level, making it impossible to determine F_0. While accurate values of F_0 can be determined by lowering the intensity of the actinic light, the subsequent fluorescence transient falls short of the maximum fluorescence level F_M. This problem can be overcome by using a continuous light source, that is controlled to provide low irradiance to determine F_0, and saturating irradiance to determine F_M (e.g., Oxborough and Baker, 1997b and Baker et al., 2001; also see Oxborough and Baker, and Oxborough, this volume). However, the fluorescence signals must be normalized using a long exposure time for measurements of F_0, and a short exposure time for measurements of F_M. Oxborough and Baker (1997b) accomplished this by keeping the number of incident photons constant during each exposure and image integration period. A similar approach was used earlier (Genty and Meyer, 1994) to measure F_S and F'_M fluorescence levels in leaves of *Phaseolus vulgaris* and *Xanthium strumarium*.

In some applications a continuous light source is adequate. For example, microscopic imaging of steady state fluorescence parameters can be done using a continuous laser source (Hoque and Remus, 1994; Gunning and Schwartz, 1999; Mehta et al., 1999; Vácha et al., 2000). Moya et al. (1998) used sunlight to excite fluorescence in leaves, but did not attempt to capture images. They distinguished the fluorescence signal from scattered sunlight by using the dark Frauenhofer lines of the solar spectrum at 687 and 760 nm.

2. Modulated Light Sources

A major advancement in non-imaging fluorometry was the introduction of modulated measuring light sources, which greatly enhanced the dynamic range of Chl fluorescence measurements over a wide range of actinic light intensities (Schreiber et al., 1986; see Schreiber, this volume). The first use of modulated light excitation for imaging Chl fluorescence from a leaf used flashes produced by a xenon lamp (Fenton and Crofts, 1990). Today light-emitting diodes (LEDs) offer a more versatile modulated light source. In contrast to discharge flash-lamps, the duration of the flashes from LEDs can be controlled down to the sub-microsecond range and light levels can be controlled from low light to instantaneous irradiances exceeding sun light by as much as two orders of magnitude (Nedbal et al., 1999). Current technology offers very powerful red and orange diodes, and the emission range is rapidly expanding towards blue and ultraviolet bands. Flashing panels of light emitting diodes were used to capture fluorescence images of plants in Nedbal et al. (2000a,b). The short measuring flashes from LEDs allow an accurate determination of F_0 images, which to our knowledge cannot be accomplished by any other imaging technology (for a discussion, see Bowyer et al., 1998). Sub-millisecond LED flashes have also been used to capture images of delayed fluorescence[6] from algal cultures (Bennoun and Béal, 1997).

Although it is technically challenging, modulated measuring light can be used to measure fluorescence signals of leaves in direct sunlight under field conditions. Fluorescence imaging of leaves in sunlight is difficult because the solar spectrum overlaps the Chl emission spectrum. Sunlight and Chl fluorescence can be separated using for excitation intense flashes in an expanded beam from Raman shifted, tripled-frequency Nd-YAG laser at 397 nm (Edner et al., 1994; Johansson et al., 1996) or from tripled-frequency Nd-YAG laser pulsing at 355 nm (Lichtenthaler and Miehé, 1997; Buschmann and Lichtenthaler, 1998). This technique is known as multi-color imaging because in addition to imaging Chl fluorescence, the Nd-YAG laser driven instruments detect emission in the blue and green spectral region (Buschmann et al., 2000). Recently modulated laser beams have been used to image Chl fluorescence lifetimes. Holub et al. (2000) used a laser beam modulated at 80 MHz to image Chl fluorescence lifetimes of leaves and individual cells of maize, *Arabidopsis*, and cells of *Chlamydomonas reinhardtii*. Microscopic images of Chl fluorescence lifetimes of green microalgae have been recorded using picosecond laser flashes by König et al. (1998).

B. Detectors

Although fluorescence images of plants can be captured by conventional photography, the analysis is limited to static images (Björn and Forsberg, 1979; Gibbons and Smille, 1980; Yanase and Andoh, 1992; Jensen and Siebke, 1997). This has changed with the introduction of CCD cameras, which provide dynamic images of Chl fluorescence that can be digitized and transferred to a computer. CCD cameras operate by capturing light in a two-dimensional array of photosensitive sites that are associated with the pixels (picture elements) of the final image. A typical CCD camera consists of an orthogonal array (hexagonal arrays have become available recently) of 700 × 400 elements. The working cycle of a CCD camera begins by conversion of photons into charge pairs at the Si-SiO_2 interface of the photosensitive sites. For red light the quantum yield of the conversion process is about 40% in front-illuminated CCD chips, and nearly 90% in back-illuminated CCD chips. The signal-to-noise ratio is limited by the number of photons incident on each site, during the integration time. The number of photoelectrons can be increased by lengthening the integration time, which in a typical low cost CCD video camera is maximally in the range of tens of milliseconds (Daley, 1995). The integration time can be lengthened even further to improve imaging of low intensity signals (Oxborough and Baker, 1997b). However, unless the CCD chip is cooled, the long integration times result in accumulation of a significant

[6] Also referred to as delayed light emission. See Tyystjärvi and Vass, this volume for details.

dark signal (Bennoun and Béal, 1997; Oxborough and Baker, 1997b). The dark signal problem can be overcome by operating the CCD chip at a very short integration time (a few microseconds) (Nedbal et al., 2000a; Küpper et al., 2000). However, this requires highly sensitivity chips to accumulate sufficient charge during the brief integration time.

Charge coupled device chips are analog devices that operate by integrating the incoming light signal simultaneously at each photosensitive site. The number of electric charges at each site is proportional to the number of photons incident on the site during the integration period. The charge stored at each site must be read and recorded. In contrast to image capture, the photosensitive sites are read in series by shifting the charge between neighboring sites towards a read-out register. Serial transfer and reading is a relatively slow process and adds read-out noise to the signal. Reading time is the limiting factor in the frequency at which a CCD camera can capture images. Low cost CCD cameras are limited to capture rates of about 25 full frames per second. More expensive progressive scan CCD chips can work faster by reading selected lines of pixels instead of full frames, thus increasing the imaging capture rate. The image capture rate can be increased by the use of CMOS (Complementary Metal Oxide Semiconductor) array detectors, which are designed to read each photosensitive site independently, obviating the need to transfer electrons from one site to another. CMOS technology has the added advantages of lower production costs and the chips can be designed to allow each photosensitive site to be directly connected to other electronic components. However, the sensitivity of CMOS detectors has been, until recently, significantly lower than CCD chips, which limited their usefulness for chlorophyll fluorescence imaging applications.

Adding an image intensifier can increase the sensitivity of imaging CCD cameras[7]. An image intensifier depends on a microchannel plate in which photoelectrons are multiplied in each channel (analogous to signal amplification in a photomultiplier). At the end of each channel, photoelectrons strike a phosphorus layer, resulting in a light flash that is detected by a CCD chip. This technique has been successfully used for microimaging (Takahashi et al., 1994; König et al., 1998) and for rapid image capture in synchrony with the rapidly modulated excitation light (Holub et al., 2000). Image intensifiers, gated at 20 ns intervals, have been also used to eliminate the background signal originating from sunlight in multi-color fluorescence imaging applications (Edner et al., 1994; Johansson et al., 1996; Lichtenthaler and Miehé, 1997; Buschmann and Lichtenthaler, 1998). König et al. (1998) used image intensification to achieve ultra-fast image capture based on 200 ps gating times.

In another novel application, Simon-Blecher et al. (1996) combined a CCD camera with an interferometer to obtain spectrally resolved fluorescence images. This system would be useful when spectral differences are expected due to differences in pigment concentration, such as in algal and cyanobacterial communities growing on ocean corals.

C. Data Handling

Willard Boyle and George Smith originally developed the CCD chip at Bell Labs in 1969 for computer data storage. In 1974, Fairchild Electronics used the chip to produce the first imaging CCD camera. The information stored at each photosensitive site in a chip typically consists of tens of thousands of electrons, representing up to a 16 bit number, or 65,536 levels. However, depending on the digitization process, the actual read-out resolution is typically a 12 or 8 bit number, representing 4096 levels, or 256 levels, respectively. A hallmark of imaging analysis is the enormous amount of information that must be transferred and stored. Images captured by CCD chip with 700 × 400 photosensitive sites, at a frequency of 25 images/s and digitized at 8-bit resolution, fills 7 megabytes of computer memory per second. Instruments that operate at a higher resolution, or include additional spectral information (Edner et al., 1994; Johansson et al., 1996; Lichtenthaler and Miehé, 1997; Buschmann and Lichtenthaler, 1998) are even more demanding on information transfer technology.

Fluorescence images are stored in the computer in data fields that represent all photosensitive CCD elements for each image captured during a measurement. After storage, software tools are used to divide the information into useful image segments. For example, data may be segmented based on a fluorescence signature, such as DCMU-inhibited or fully active regions as shown in Fig. 2A. The user may select individual bacterial or algal colonies, or individual plants for mutant screening (Gibbons and Smille, 1980; Fenton and Crofts, 1990; Bennoun and Béal,

[7] Similar to those used in night vision devices

1997; Niyogi et al., 1997, 1998; Shikanai et al., 1998; Peterson and Havir, 2000; Varotto et al., 2000; also see Niyogi et al., this volume). In precision farming, segmentation tools are being developed to distinguish between crop and weed plants by combining information on fluorescence emission with plant topology. Segmentation can be done manually or automatically (for example, based on highly contrasting features in neighboring segments as shown for non-photochemical quenching in Fig. 2A). Once data segmentation has been completed, all the pixels within a selected region are integrated to give an average value at any given time. These average values are then used to plot characteristic fluorescence parameters as a function of time. For example, integration of fluorescence signals over an area with low non-photochemical quenching (Fig. 2A) revealed which regions of the leaf were inhibited, and provided the quantitative data used for plotting fluorescence emission due to DCMU inhibition (Fig. 2B).

The last step in fluorescence imaging is data presentation in a format that allows visualization of the fluorescence parameters of interest. This is a challenging task that depends on the resolution of the instrument, software design, and limitations imposed by the human eye (the average person can discriminate about 200 levels of gray, which is less than 8-bit resolution). A common technique to enhance contrast is to use the visible spectrum of sunlight as a scale, in which blue represents the lowest signals and red represents the highest signals (the spectrum is typically divided into 256 levels (e.g., Fig. 2A, top row). However, when the signal of interest spans a small fraction of the 256 levels available in an 8-bit resolution instrument the differences are difficult to see (e.g., see the histogram of F_V/F_M shown in Fig. 2C). The contrast can be increased by re-scaling the colors, so that blue-to-red spectrum is used to cover a small range of the entire parameter range. However, rescaling means that images using different color scales cannot be compared. Another technique to enhance visual perception of imaged data is to use 3-dimensional presentations, in which signal levels are indicated not only by the blue-red spectral colors, but also by the height of each element (Fig. 3).

D. Experimental Protocols

In many applications, the experimental protocols developed for non-imaging fluorometry can be adapted to imaging fluorometers with little modification. An example are the protocols for measuring fluorescence levels in saturating light (F_M, F_M'), which were adapted to imaging fluorometry (Balachandran et al., 1994; Rolfe and Scholes, 1995; Oxborough and Baker, 1997b; Osmond et al., 1998), yielding two-dimensional maps of Stern-Volmer non-photochemical quenching NPQ = $(F_M - F_M')/F_M'$. When combined with measurements of steady-state fluorescence for light-adapted leaves (F_S), the maximum fluorescence measurements (F_M') can be used to estimate the apparent quantum efficiency of Photosystem II $\phi_{PS\ II} = (F_M' - F_S)/F_M')$. The apparent quantum efficiency of PS II ($\phi_{PS\ II}$) can be used to map estimates of the instantaneous quantum yield of CO_2 fixation over the surface of a leaf (Genty and Meyer, 1994; Rolfe and Scholes, 1995; Siebke and Weis, 1995a; Oxborough and Baker, 1997b; Baker et al., 2001). It should be noted that to map the rate of CO_2 fixation over the surface of a leaf, the quantum yield determined by fluorescence must be multiplied by the absorbed light energy (Krall and Edwards, 1992). A method for estimating absorbed light energy using imaging technology is discussed in Section II.F.

However, for other applications, developing protocols for imaging chlorophyll fluorescence parameters presents unique challenges. For example, there are technical limitations associated with imaging the relatively low levels of F_0 and of F_0' (discussed by Bowyer et al., 1998). Another problem is the difficulty of generating light pulses that are saturating over the entire sample surface, which is necessary to map F_M and of F_M' (discussed in Section II.E). Several strategies have been developed to overcome these limitations. For example, F_M has been approximated by the peak fluorescence, F_P, measured in high, but sub-saturating, actinic light (Balachandran et al., 1994; Ning et al., 1995, 1997). Ning et al. (1995) substituted the steady-state fluorescence level measured in low intensity actinic light (F_S) for F_0 in calculating fluorescence parameters. Fenton and Crofts (1990) approximated F_0 by using the initial fluorescence level measured during the first integration period in a moderately intense actinic light. In some applications, a fixed ratio between F_M and either F_0 or F_0' was assumed in order to estimate the non-photochemical quenching coefficient qN. Examples include: $q_N \approx (F_M - F_M')/0.8FM$ (Daley et al., 1989), $q_N \approx (F_M - F_M')/0.775F_M$ (Siebke and Weis, 1995a), and $q_N \approx (F_M - F_S)/0.8F_M$ (Cardon et al., 1994). In some applications, quantitative values were determined by parallel measurements of imaging and non-imaging fluorometry (Daley et

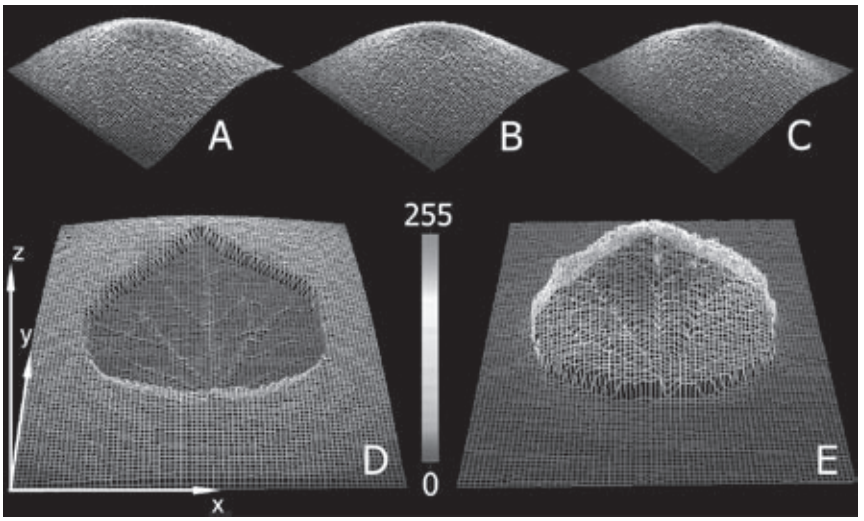

Fig. 3. Three-dimensional visualization of signals imaged by a CCD camera. The two-dimensional image is represented by the x-y axes and the signal amplitude is represented by the z-axis. A red-blue color scale (for color images see the color section of this volume) is used to enhance visual perception, with high signals shown in red (maximum 255) and low signals in blue (minimum 0). (A) Fluorescence signal of a plastic sheet containing a uniformly distributed fluorescent dye (Nile Blue) illuminated by diffuse homogenous light. The non-uniformity of the image is due to the close proximity of the camera objective lens, which is located 9 cm above the Nile Blue sheet. (B) Fluorescence signal emitted by the Nile Blue sheet excited by measuring flashes from an array of orange light emitting diodes (λ_{max} = 635 nm). The non-uniformity of the signal is due to the camera optics (shown in Fig. 2A) and non-uniformity of the measuring light field. (C) Fluorescence signal emitted by the Nile Blue sheet excited by an intense pulse of light from a 250 W halogen lamp (3000 μmol(photons) m^{-2} s^{-1}). The non-uniformity of the signal is due to the combined effect of the camera optics and inhomogeneity of the actinic light field. (D) Scattered light signal from a leaf (*Hedera*) placed on white paper that was illuminated by the orange LED array. Scattered light was selected by placing an orange filter in front of the camera. The low signal in the center of the image is due to light absorption by the leaf. (D) Image of the fluorescence signal emitted by the leaf excited by the orange LED array. Fluorescent light was selected by placing a red filter in front of the camera that passed 695–750 nm light. The camera sensitivity was adjusted to provide similar signal amplitude in each experiment. Further details are given in the text.

al., 1989; Peterson and Aylor, 1995; Shikanai et al., 1998; Peterson and Havir, 2000).

In many applications, such as screening for mutants or identifying infected leaf areas, qualitative measurements are sufficient for selection decisions. Images of the fluorescence decrease ratio, $R_{Fd} = (F_M - F_S)/F_M$ (Lichtenthaler and Miehé, 1997; Lichtenthaler and Babani, 2000), or $Y' = (F_M - F_S)/F_M$, an empirical estimate of the quantum yield (Ning et al., 1995), can be used to identify local effects of biotic or abiotic stress without having to determine F_0 and F_0'. Peterson and Havir (2000) screened for *Arabidopsis* mutants deficient in non-photochemical quenching using an empirical imaging parameter that compared steady-state fluorescence of seedlings measured in air, and in CO_2-free air containing 5% O_2.

With the development of more advanced instrumentation and new theoretical approaches, accurate quantitative determinations are now becoming available for Chl fluorescence parameters that have been, until recently, beyond most imaging applications. Among the critical parameters required for robust quantitative analysis are F_0 and F_0'. Oxborough and Baker (1997a) developed a model to calculate the F_0' image based on measured images of F_0, F_M, and of F_M'. Oxborough and Baker (1997b) and Nedbal et al. (2000a) have both constructed instruments that can image low F_0 fluorescence levels. The imaging fluorometers described in Nedbal et al. (2000a) and in Küpper et al. (2000) are conceptually similar to the pulse-amplitude-modulated (PAM) fluorescence technique that is commonly used in non-imaging experiments. The introduction of modulated-light imaging allows analysis based on fluorescence relationships, including F_0 , that greatly increases the usefulness of imaging fluorometry for basic research as well as for applications in biotechnology. An example is in imaging of Chl fluorescence from ripening lemons (Nedbal et al., 2000b). It was found that the most useful parameter to distinguish

between mold-infected and healthy lemon peel is the ratio F_0/F_V. Analysis of *Brassica* leaves exposed to destruxins showed that images of F_0/F_V also provided a high contrast between infected and healthy leaf areas (Soukupová et al., 2003).

Recently, technology has been developed that enables imaging of fluorescence lifetimes using rapidly modulated laser light and imaging detectors (König et al., 1998; Holub et al., 2000). The introduction of a new generation of microchannel-plate photomultiplier detectors should advance the sensitivity and time resolution of fluorescence lifetime imaging instruments (Kemnitz et al., 1997).

E. Technical Limitations

Although the performance gap between imaging and non-imaging fluorometers is narrowing due mainly to improved light sources and detectors, significant limitations remain. One of the major technical challenges is producing a uniform light field over a large sample area at a reasonable cost. Heterogeneity in measuring and actinic light fields can compromise data interpretation and is especially important for applications that require quantitative analysis. In some cases, measuring irradiance heterogeneity can be overcome by limiting analysis to the ratios of two fluorescence images, e.g., $(F_M–F_M')/F_M$. However, this approach does not correct for the unavoidable variation in kinetics induced by heterogeneous actinic irradiance. The best solution is to design a light system that provides uniform measuring and actinic light fields. However, because of technical limitations and increased costs, it is difficult to provide saturating light over a large area. As a consequence, most imaging measurements of the maximum fluorescence (F_M or F_M') have been limited to relatively small areas. Mapping F_M images of a leaf requires light intensities of 2,000 to 10,000 μmol photons/m^2 s that must be sustained for about a second. An approximate calculation based on black body radiation indicates that an ideal 500 W incandescent lamp, operating at 5,000 K, would provide a maximum of 2,200 μmol photons/m^2 s of photosynthetically active radiation over a 42 × 42 cm square. In practice, the actual intensity would be lower because the efficiency of the lamp and collecting optics are far from ideal. In addition, it is difficult to project incandescent light uniformly over a large area. To achieve the largest possible area of saturating light for a given source, the light field should be as uniform as possible, so that hot spots (light intensities that exceed saturation) or cold spots (light intensities below saturation) are avoided. In practice, photon fluxes used for F_M imaging have ranged from 0.228 μmol photons/s (Daley et al., 1989) to 4.5 μmol photons/s (Genty and Meyer, 1994 and Nedbal et al., 2000a). These low flux densities limit the sample area, which in the examples cited above ranged from 0.64 cm^2 to 25 cm^2.

Lootens and Vandecasteele (2000) avoided the use of incandescent light sources by irradiating with intense stroboscopic lamps. Alternatively to incandescent or stroboscopic light sources, steadily increasing power of LED light sources makes them practical in generating relatively strong irradiance over a large area (www.psi.cz, www.qubitsystems.com)[8].

To reliably interpret quantitative fluorescence imaging data, it is important to determine the uniformity of the illuminating light field. This can be done using the CCD camera of the imaging instrument. However, this technique must take into account the fact that CCD cameras are not optically perfect and may produce images significantly affected by limited peripheral sensitivity. Figure 3A shows a pseudo 3-D presentation of the fluorescence emission of a homogeneous layer of a fluorescent dye (Nile blue) excited by a distant light source arranged to provide homogeneous diffuse light. The image is clearly heterogeneous, revealing seemingly higher fluorescence level in the center of the field. The heterogeneity is caused by the optics of the camera and depends on the distance of the camera from the sample (in this case 9 cm). The fluorescence surface shown in Fig. 3B was obtained with the same dye layer, but was excited directly by panels of orange LEDs (Nedbal et al., 2000a). The curvature of the 3-dimensional presentation is slightly greater than that seen in Fig. 3A because of heterogeneity in the measuring light. A map of the light field determined using a Licor quantum sensor showed that the intensity was homogeneous over the area of a Petri dish (64 cm^2) within ±7%. Generating a uniform light field at an intensity sufficient to measure F_M and F_M' is even more difficult. The irradiance must be several thousands of μmol photons/m^2 s, last for a second or so, and switch on and off within a few milliseconds. Fig. 3C shows the irradiance field provided by a 250 W halogen lamp equipped with a low pass 650 nm dichroic mirror.

[8] An array of orange HLMP-EH08 (Agilent Technologies, Palo Alto, CA, USA), can generate ca. 300 to 400 μmol photons/m^2 s of unfiltered light in a distance of 10 cm when electrical current of 30 mA is used in each LED.

The light field was uniform within ± 12% over a the surface of a Petri dish at an irradiance of 3000 μmol photons/m^2 s.

F. Impact of Scattering, Absorption, and of Re-Absorption of Fluorescence

Leaves can absorb over 90% of incident sunlight, creating a strong internal light gradient in which cells located near the top of the leaf may be operating in saturating or super-saturating irradiance, while cells deeper in the leaf are operating under sub-saturating irradiance. How deeply light penetrates a leaf depends on the wavelength and angle of the incident light, and on the structure and optical properties of the leaf. Because Chl strongly absorbs red and blue light, fluorescence images induced by red or blue measuring light view cells at or near the top of the leaf. In contrast, green, yellow, or orange light penetrates more deeply into the leaf, providing fluorescence images of cells located deeper in the leaf. As a consequence, leaf images of Chl fluorescence typically sample a relatively narrow band of cells located in, or slightly below, the top of the leaf. This can be a significant limitation in leaf imaging, particularly in efforts to extrapolate whole leaf activity from imaging data. A more accurate picture of leaf activity can be attained by analyzing images produced using different measuring light wavelengths, different incident angles, and imaging both the top and bottom surfaces of the leaf.

Another factor that can be important in analyzing imaging data is reabsorption of Chl fluorescence by Chl molecules in the same or the neighboring cells. The reabsorption effect is mainly due to the fact that fluorescence emitted by Chl in the cells located below the surface of the leaf must pass through upper cells before being detected. The Chl in the upper cells acts as a filter, absorbing in the red-band of the Chl fluorescence emission spectrum.

With minor modification a fluorescence-imaging instrument can be used to map the relative amount of light absorbed by leaf. The technique depends on removing the red filters normally placed in front of the CCD camera. With the filters removed the camera is used to image scattered light from a leaf placed on a white surface that is selected to scatter light uniformly. Figure 3D shows, in a 3-dimensional representation, an image of scattered light from a Hedera leaf placed on white paper. The minimum signal is due to the highly absorbing Chl-rich areas of the leaf, while the maximum signal is due to light scattering by the white paper. The difference between the intensity of light scattered by the leaf, and the intensity of light scattered by the white paper surface around the leaf, is a measure of the amount of light absorption by the leaf. Figure 3E shows fluorescence image of the same leaf captured with the red filters in place. The low signal from the white paper indicates that scattered light is negligible in the captured signal. This technique provides a method to improve estimates of photosynthetic rates over the surface of the leaf based on Chl fluorescence imaging, which require a map of the quantum yield and a map of the amount light absorbed by the leaf (Krall and Edwards, 1992).

The method for mapping Chl absorption in a Hedera leaf that contained light-green veins and dark interveinal areas is shown in Fig. 4. Images of scattered light were obtained by removing the red filter from the camera. Note that the light scattered from a highly scattering white paper (Fig. 4C) was reduced after the filter was placed before the camera objective (Fig. 4D). The relative decrease in the scattered signal can be used to map the leaf absorption of the measuring light (in Fig. 4F). Figure 5 shows a comparison of standard fluorescence images of F_0, F_M, F_v, and F'_M emission (top row), with the images that have been corrected using the absorption image shown Fig. 4F. Comparison of the top and bottom rows in Fig. 5 reveals significant difference between the two methods. For example, in the uncorrected image of F_0 (top), the relative intensity of light is lower in veins compared to the surrounding tissue, whereas in the corrected F_0 image (bottom) the fluorescence is higher in the veins than in the surrounding tissue. The same applies to the maximum fluorescence F_M. Although the veins contain less Chl than the surrounding areas, they exhibit a higher fluorescence yield because there is less re-absorption of fluorescence.

Another dimension adding complexity to the fluorescence imaging is the non-uniform absorption of the photosynthetically active irradiance along the depth profile of the leaf. The surface leaf cell layers are exposed to full incident irradiance whereas the deeper cell layers are 'enjoying' reduced photon flux density with dominating green photons. The uneven distribution of light absorption can be mapped by various techniques (Vogelmann et al., 1996) and chlorophyll fluorescence microscopy has a significant application potential in this area.

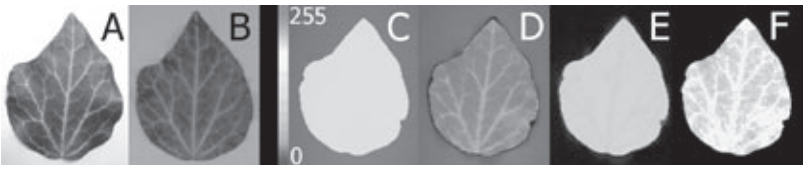

Fig. 4. Scattered light and fluorescence images of a *Hedera* leaf (for color images see the color section of this volume). (A) Color photograph of the leaf illuminated by white light (24 bit, 2048 × 1536 pixels); (B) Color photograph of the leaf illuminated by the orange LED measuring flashes (635 nm). (C) Map of scattered measuring light (635 nm) from white paper without the leaf. Note that the scattered light signal is shown only for the area previously occupied by the leaf. The image was captured without a red filter in front of the camera. (D) Map of scattered measuring light from the leaf (same as C except with the leaf). (E) The difference between images (C) and (D), showing the decrease in scattering due to light absorption by the leaf. (F) Map of the fraction of measuring light absorbed by the leaf (calculated by dividing the pixel data in image (D) pixel data in image (C). Images C-F were captured using a monochrome CCD camera (8-bit, 400 × 300 pixels).

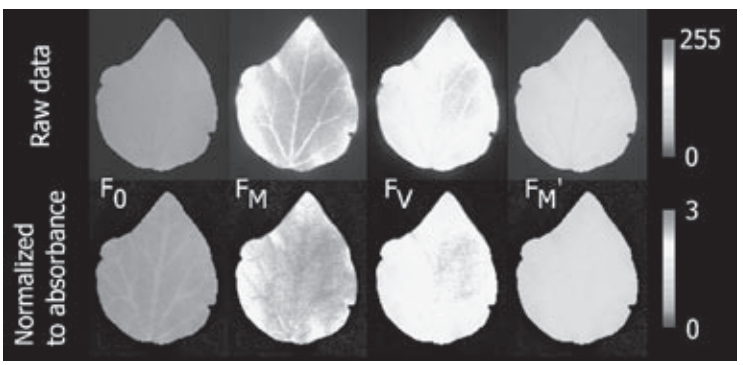

Fig. 5. Fluorescence images of F_0, F_M, F_V , and F_M' emitted by a *Hedera* leaf (top row). The bottom row shows the same fluorescence images after normalization by dividing each pixel by the value of the corresponding pixel in the image mapping the absorbed light shown in Fig. 4E. Normalization serves to correct for heterogeneity in the distribution of chlorophyll in the leaf and heterogeneity in the measuring light field, which yields a more accurate map of the fluorescence yield parameters. For color images see the color section of this volume.

III. Sources of Heterogeneity in Fluorescence Images

A. Biotic Stress

Imaging fluorometry can reveal the time course and pathway of pathogen invasion in a leaf, which makes it an effective tool for detecting early stages of viral, bacterial, and fungal infection in leaves. It is important to note that the fluorescence parameter best suited for evaluating damage depends on the type of infection; there is a better chance of detecting and assaying infected areas with more versatile imaging instruments. An example of this is provided by crown rust (*Puccinia coronata*) in oat leaves. During early stages of the disease, images of infected leaves showed only slight changes in the quantum yield of PS II, whereas non-photochemical quenching decreased substantially (Scholes and Rolfe, 1996). Similarly, leaf infection by a mosaic virus was most clearly imaged by changes in non-photochemical quenching (Osmond et al., 1998; Lohaus et al., 2000). In contrast, invasion of bean leaves by rust (*Uromyces appendiculatus*) was revealed by changes in the fluorescence induction kinetics (Peterson and Aylor, 1995). Cedar needles (*Torreya taxifolia*) infected by the fungus *Pestalotiopsis* spp. were identified by an empirical estimate of quantum yield $Y' = (F_M - F_S)/F_M$ (Ning et al., 1995), which was also used to visualize impact of phytotoxins on a hibiscus leaf (*Hibiscus sabdariffa*) (Bowyer et al., 1998). Mosaic virus (TMV) infection of tobacco caused a patchy variability in the ratio $(F_P - F_S)/F_P$ (Osmond et al., 1990; Balachandran et al., 1994). Imaging of the apparent quantum efficiency of PS II from chickpea leaves was used to assay the impact of a fungal pathogen from

Ascochyta rabiei that altered source-sink distribution (Esfeld et al., 1995; Weis et al., 1998).

Fluorescence imaging can detect biotic stress before visual symptoms appear. For example, Nedbal et al. (2000b) showed that images of Chl fluorescence of lemons provided an early warning of areas infected by *Penicillium digitatum*. This study shows the potential for using Chl fluorescence imaging to identify infected fruit so they can be removed before healthy fruit become contaminated. The effectiveness of Chl fluorescence imaging is revealed by the demonstration that images of F_0/F_V were more than 100 times more sensitive than microscopic inspection in detecting damage caused by destruxins isolated from Brassica blackspot (*Alternaria brassicae*) (Buchwaldt and Green, 1992). Further, Zangerl et al. (2002), using fluorescence imaging analysis, have shown that in wild parsnip, the impact of caterpillars eating leaves is much greater than the holes they produce.

B. Abiotic Stress

The first application of CCD technology to image Chl fluorescence investigated sunflower leaves exposed to SO_2 (Omasa et al., 1987). The images showed that fumigation induced significant and irreversible changes in fluorescence kinetics in regions of the leaf between veins, but not in regions close to veins. The authors attributed the difference to lower stomatal conductance in the regions near the veins.

As discussed in the *Introduction*, herbicide penetration into leaves is easily visualized by imaging fluorescence (Daley et al., 1989; Fenton and Crofts, 1990; Yanase and Andoh, 1992; Ning et al., 1995; Rolfe and Scholes, 1995; Lichtenthaler et al., 1997; Nedbal et al., 2000a). The inhibition pattern induced by the addition of DCMU appears in a wave-front that divides photosynthetically active and inactive regions. As is the case for biotic stress, some fluorescence parameters are more effective than others in tracking the pathway of inhibition. For example, DCMU binding has little effect on the parameters F_0 and F_M. However, the inhibition pattern can be visualized by a number of fluorescence parameters, including the kinetics of the transition from F_0 to F_M, a slowdown of the fluorescence decrease normally seen in the later phase of fluorescence induction (Ning et al., 1995; Lichtenthaler et al., 1997), or changes in non-photochemical quenching (as shown in Fig. 2B).

Images of leaves that are drought-stressed reveal a heterogeneous pattern in Chl fluorescence quenching (Lang et al., 1996; Jensen and Siebke, 1997; Meyer and Genty, 1999; Osmond et al., 1999b; Barták et al., 2000; Lichtenthaler et al., 2000). Meyer and Genty, 1999 observed a reduction in the ratio of $(F'_M - F_S)/F'_M$, in drought-stressed leaves, which they attributed to an inhibition of photosynthetic activity induced by heterogeneous stomatal closure. To develop fluorescence imaging for remote sensing, Ning et al. (1995) showed that fluorescence images captured at a distance of seven meters could effectively identify early effects of freeze damage, herbicide effects, and fungal infections. In a spectral analysis of images of tobacco leaves that included fluorescence from sources other than Chl, Lang et al. (1996) found that water-stress, combined with high-temperature stress, altered the ratio of steady-state blue, green, red, and far-red fluorescence (blue and green fluorescence are not from Chl, see Moya and Cerovic, and Lichtenthaler and Babani, this volume, for discussion). Lang and co-workers proposed that multi-color analysis could provide a simple and effective tool for early detection of various stress factors. Heisel et al. (1996) demonstrated that multi-color fluorescence imaging of maize is effective in detecting N and Fe deficiencies, but was less effective in detecting Mg and Zn deficiencies. Recently, Mazza et al. (2000) compared images of Chl fluorescence emission excited in the ultraviolet, UV-B, and blue spectral regions to estimate changes in UV-screening pigments induced by pre-exposure of soybean leaves to UV-B radiation.

C. Physiology

A number of techniques indicate that photosynthetic performance in leaves can exhibit considerable variation even in the absence of significant stress factors. One of the clearest examples is heterogeneity in stomatal aperture that gives rise to 'stomatal patchiness.' Fluorescence imaging can identify leaf regions in which the stomatal aperture is significantly below the average stomatal aperture of the leaf. The heterogeneity in stomatal conductance is dynamic and leads to local variations in the internal CO_2 concentration that is a major factor in controlling the net rate of CO_2 assimilation, and, which in turn controls steady-state levels of fluorescence emission and fluorescence quenching (Daley et al., 1989). Patchy stomata responses can be induced by low humidity, which induces dynamic changes in non-photochemical quenching (Mott et al., 1993; Cardon et al., 1994; Eckstein et al., 1996), or by infiltration

of leaves by abscisic acid (Meyer and Genty, 1998). Bro et al. (1996) used fluorescence imaging to investigate stomatal limitation together with asynchronous limitation of intrinsic metabolism following a period of dark adaptation. Fluorescence imaging also reveals significant heterogeneity in developing leaves. Young leaves of tobacco exhibit heterogeneity in fluorescence emission (Weis et al., 1998), as do cucumber leaves during development and expansion (Croxdale and Omasa, 1990a, b).

Another example of physiological heterogeneity in leaves is the oscillations observed in assimilatory activity. K. Siebke and E. Weis have induced photosynthetic oscillations in $(F'_M - F_S)/F'_M$ images in heterobaric leaves of *Glechoma hederacea* by step changes in O_2 and CO_2 concentrations (Siebke and Weis, 1995a) and by step changes in the light intensity (Siebke and Weis, 1995b). Images of harmonically forced oscillations in fluorescence emission were proposed to map regulation in light capture by Nedbal and Brezina (2002). Chlorophyll fluorescence imaging was also used to reveal dynamic oscillatory heterogeneity of ϕ_{PSII} over surface of CAM plant *Kalanchoe daigremontiana* as it occurs in circadian rhythm (Rascher et al., 2001). It is noteworthy that the oscillations in fluorescence emission could sometimes only be detected by imaging analysis, because they occur at different frequencies and phases in different leaf regions. In non-imaging fluorescence measurements, which effectively measures an average fluorescence signal over the sample area, and in other integrative methods, such as gas exchange measurements, the oscillations are damped out due to multiple phases of the oscillations in different leaf segments. This effect can be avoided by microscopic imaging, which reveals spontaneous oscillations of fluorescence emission with single cells oscillating at different frequencies and phases (Ferimazova et al., 2002).

D. Mutations

Beginning with the work of Garnier (1967), Bennoun and Levine (1967) and Bennoun and Béal (1997) in which they imaged Chl fluorescence by photographic and visual analysis to select photosynthetic mutants of algal colonies, the use of chlorophyll fluorescence imaging to screen for mutants has become ubiquitous (Miles and Daniel, 1973; Gibbons and Smille, 1980; Fenton and Crofts, 1990). Recent examples include the work of K. Niyogi and coworkers who developed a sophisticated image analysis to select for mutants deficient in non-photochemical quenching in algae (Niyogi et al., 1997) and in *Arabidopsis* (Niyogi et al., 1998; Shikanai et al., 1998; Peterson and Havir, 2000), and Kruse et al. (1999), who used the technique to find state-transition mutants of green alga *Chlamydomonas reinhardtii*. Bennoun and Béal (1997) used parallel imaging of Chl fluorescence and delayed fluorescence (also called delayed luminescence, or delayed light emission; see the chapter by Tyystjärvi and Vass, this volume) to identify algal mutants affecting the electrochemical gradient across the photosynthetic membrane.

IV. Future Applications

Since Kautsky and Hirsch (1931) first visualized the fluorescence emission from leaves and Omasa et al. (1987) constructed the first CCD camera imaging fluorometer, the technique of Chl fluorescence imaging has evolved into a ubiquitous tool for determining the underlying molecular and physiological mechanisms that determine photosynthetic rates and efficiencies. This knowledge, combined with technical advancements, is opening the way for a variety of applications in plant research and biotechnology, including high throughput screening for mutants, and detection and identification of biotic and abiotic stress factors. Although currently the use of fluorescence imaging for screening mutants is constrained by small sample areas, improvements in light sources can be expected to greatly increase throughput over the next few years. Increased throughput rates will require more robust and sophisticated tools for image segmentation and analysis that can benefit from systems incorporating artificial intelligence (Tyystjärvi et al., 1999). Improved modulation of measuring light systems and increased sensitivity of image detectors should enable measurements of crop plants in the field in full sunlight. This would make fluorescence imaging an important component in precision farming systems. Imaging instruments are currently being developed to measure fluorescence dynamics from distances of several meters (Ning et al., 1995; Lichtenthaler et al., 1996; Johansson et al., 1996; see Moya and Cerovic, this volume). The field imaging fluorometers can be expected to perform at the same level as the PAM (Pulse Amplitude Modulation) non-imaging fluorometry, thereby providing monitoring of drought, heat, chilling, photoinhibition, and

nutrient depletion in crop plants. Novel applications of fluorescence imaging include the non-invasive analysis of lichen, algal and cyanobacterial growth on stone statues, historical monuments, and ancient cave formations (Jensen and Siebke, 1997). In food technology, Chl fluorescence imaging can provide a rapid and non-invasive, post-harvest evaluation of the quality of fruits and vegetables (e.g., DeEll et al., 1995; Gandul-Rojas et al., 1999; Nedbal et al., 2000b; DeEll and Toivonen, 2000), and of seeds (Jalink et al., 1998). On the microscale, fluorescence imaging is being used to map fluorescence parameters of individual cells or even chloroplasts (Küpper et al., 2000; Baker et al., 2001; Ferimazova et al., 2002). On a global scale, fluorescence imaging will be playing an increasingly important role in monitoring the impact of atmospheric and global climate change on native ecosystems.

Acknowledgments

L. N. was supported in part by a grant LN00A141 of the Czech Ministry of Education and by AV0Z6087904 project of Institute of Landscape Ecology CAS. Photon Systems Instruments provided FluorCam instrument (www.psi.cz) that captured most of the images shown in this Chapter. Critical reading by Barry Osmond and Govindjee is appreciated.

References

Baker N, Oxborough K, Lawson T and Morison J (2001) High resolution imaging of photosynthetic activities of tissues, cells and chloroplasts in leaves. J Exp Bot 52: 615–621

Balachandran S, Osmond C and Daley P (1994) Diagnosis of the earliest strain-specific interactions between tobacco mosaic virus and chloroplasts of tobacco leaves in vivo by means of chlorophyll fluorescence imaging. Plant Physiol 104: 1059–1065

Barták M, Hájek J and Gloser J (2000) Heterogeneity of chlorophyll fluorescence over thali of several foliose macrolichens exposed to adverse environmental factors: Interspecific differences as related to thallus hydration and high irradiance. Photosynthetica 38: 531–537

Bennoun P and Levine RP (1967) Detecting mutants that have impaired photosynthesis by their increased level of fluorescence. Plant Physiol 42: 1284–1287

Bennoun P and Béal D (1997) Screening algal mutant colonies with altered thylakoid electrochemical gradient through fluorescence and delayed luminescence digital imaging. Photosynth Res 51: 161–165

Bilger W and Björkman O (1990) Role of the xanthophyll cycle in photoprotection elucidated by measurements of light-induced absorbance changes, fluorescence and photosynthesis in leaves of *Hedera canariensis*. Photosynth Res 25: 173–185

Björn L and Forsberg A (1979) Imaging by delayed light emission (phytoluminography) as a method for detecting damage to the photosynthetic system. Physiol Plantarum 47: 215–222

Bowyer W, Ning L, Daley L, Strobel G, Edwards G and Callis J (1998) In vivo fluorescence imaging for detection of damage to leaves by fungal phytotoxins. Spectroscopy 13: 36–44

Bro E, Meyer S and Genty B (1996) Heterogeneity of leaf CO_2 assimilation during photosynthetic induction. Plant Cell Environ 19: 1349–1358

Buchwaldt L and Green H (1992) Phytotoxicity of destruxin B and its possible role in the pathogenesis of *Alternaria brassicae*. Plant Path 41: 55–63

Buschmann C and Lichtenthaler H (1998) Principles and characteristics of multi-colour fluorescence imaging of plants. Plant Physiol 152: 297–314

Buschmann C, Langsdorf G and Lichtenthaler H (2000) Imaging of the blue, green, and red fluorescence emission of plants: An overview. Photosynthetica 38: 483–491

Cardon Z, Mott K and Berry J (1994) Dynamics of patchy stomatal movements, and their contribution to steady-state and oscillating stomatal conductance calculated using gas-exchange techniques. Plant Cell Environ 17: 995–1007

Croxdale J and Omasa K (1990a) Chlorophyll-*a* fluorescence and carbon assimilation in developing leaves of light-grown cucumber. Plant Physiol 93: 1078–1082

Croxdale J and Omasa K (1990b) Patterns of chlorophyll fluorescence kinetics in relation to growth and expansion in cucumber leaves. Plant Physiol 93: 1083–1088

Daley F (1995) Chlorophyll fluorescence analysis and imaging in plant stress and disease. Can J Plant Pathology 17:167–173

Daley P, Raschke K, Ball J and Berry J (1989) Topography of photosynthetic activity of leaves obtained from video images of chlorophyll fluorescence. Plant Physiol 90: 1233–1238

Dau H (1994) Molecular mechanisms and quantitative models of variable Photosystem II fluorescence. Photochem Photobiol 60: 1–23

DeEll J and Toivonen P (2000) Chlorophyll fluorescence as a non-destructive indicator of broccoli quality during storage in modified-atmosphere packing. Hort Science 35: 256–259

DeEll J, Prange R and Murr D (1995) Chlorophyll fluorescence as potential indicator of controlled-atmosphere disorders in 'Marshall' McIntosh apples. Hort Science 30: 1084–1085

Eckstein J, Beyschlag W, Mott K and Ryel R (1996) Changes in photon flux can induce stomatal patchiness. Plant Cell 19: 1066–1074

Edner H, Johansson J, Svanberg S and Wallinder E (1994) Fluorescence lidar multicolor imaging of vegetation. Appl Optics 33: 2471–2479

Esfeld P, Siebke K, Wacker I and Weis E (1995) Local defense-related shift in the carbon metabolism in chickpea leaves induced by a fungal pathogen. In: Mathis P (ed) Photosynthesis: From Light to Biosphere, pp 663–666. Kluwer Academic Publishers, Dordrecht

Falkowski P and Kolber Z (1995) Variations in chlorophyll fluorescence yields in phytoplankton in the world oceans. Aust J Plant Physiol 22: 341–355

Fenton J and Crofts A (1990) Computer aided fluorescence imaging of photosynthetic systems—application of video imaging

to the study of fluorescence induction in green plants and photosynthetic bacteria. Photosynth Res 26: 59–66

Ferimazova N, Küpper H, Nedbal L and Trtílek M (2002) New insights into photosynthetic oscillations revealed by two-dimensional microscopic measurements of chlorophyll fluorescence kinetics in intact leaves and isolated protoplasts. Photochem Photobiol 76: 501–508

Gandul-Rojas B, Cepero M and Minguez-Mosquera M (1999) Chlorophyll and carotenoid patterns in olive fruits, *Olea europaea* cv. Arbequina. J Agricult Food Chem 47: 2207–2212

Garnier J (1967) Une méthode de détection, par photographie, de souches d'algues vertes émettant in vivo une fluorescence anormale. Comptes Rendus Acad Sci 265: 874–877

Genty B and Meyer S (1994) Quantitative mapping of leaf photosynthesis using chlorophyll fluorescence imaging. Aust J Plant Physiol 22: 277–284

Gibbons G and Smille R (1980) Chlorophyll fluorescence photography to detect mutants, chilling injury and heat stress. Plant Physiol 45: 269–282

Govindjee (1995) Sixty-three years since Kautsky: Chlorophyll *a* fluorescence. Aust J Plant Physiol 22: 131–160

Govindjee and Nedbal L (2000) Seeing is believing. Photosynthetica 38: 481–482

Govindjee, Amesz J and Fork D (eds) (1986) Light Emission by Plants and Bacteria. Academic Press, Orlando

Gunning B and Schwartz O (1999) Confocal microscopy of thylakoid autofluorescence in relation to origin of grana and phylogeny in the green algae. Plant Physiol 26: 695–708

Heisel F, Sowinska M, Miehe J, Lang M and Lichtenthaler H (1996) Detection of nutrient deficiencies of maize by laser induced fluorescence imaging. J Plant Physiol 148: 622–631

Holub O, Seufferheld M, Gohlke C, Govindjee and Clegg R (2000) Real-time fluorescence lifetime-resolved imaging (FLI) — a new technique for photosynthesis research. Photosynthetica 38: 581–599

Hoque E and Remus G (1994) Native and atrazine-induced fluorescence of chloroplasts from palisade and spongy parenchyma of beech (*Fagus sylvatica* L.) leaves. Remote Sens Environ 47: 77–86

Jalink H, van der Schoor R, Frandas A, van Pijlen J and Bino R (1998) Chlorophyll fluorescence of *Brassica oleracea* seeds as a non-destructive marker for seed maturity and seed performance. Seed Sci Res 8: 437–443

Jensen M and Siebke K (1997) Fluorescence imaging of lichens in the macro scale. Symbiosis 23: 183–195

Johansson J, Andersson M, Edner H, Mattsson J and Svanberg S (1996) Remote fluorescence measurements of vegetation spectrally resolved and by multi-colour fluorescence imaging. Plant Physiol 148: 632–637

Kautsky H and Hirsch A (1931) Neue Versuche zur Kohlensauerassimilation. Naturwissenschaften 48: 964–964

Kemnitz K, Pfeifer L, Paul R and Moisan C (1997) Novel detectors for fluorescence lifetime imaging on the picosecond time scale. J Fluorescence 7: 93–98

Koizumi M, Takahashi K, Mineuchi K, Nakamura T and Kano H (1998) Light gradients and the transverse-distribution of chlorophyll fluorescence in mangrove and camellia leaves. Annals Bot. 81: 527–533

König K, Boehme S, Leclerc N and Ahuja R (1998) Time-gated autofluorescence microscopy of motile green microalga in an optical trap. Cell Mol Biology 44: 763–770

Krall J and Edwards G (1992) Relationship between Photosystem-II activity and CO_2 fixation in leaves. Physiol Plantarum 86: 180–187

Kramer D and Crofts A (1996) Control and measurement of photosynthetic electron transport in vivo. In: Baker N (ed) Photosynthesis and the Environment, pp 25–66. Kluwer Academic Publishers, Dordrecht

Krause G and Jahns P (2002) Pulse amplitude modulated chlorophyll fluorometry and its application in plant science. In: Green BR and Parson WW (eds) Light Harvesting Antennas, pp 373–399. Kluwer Academic Publishers, Dordrecht

Kruse O, Nixon P, Schmid G and Mullineaux C (1999) Isolation of state transition mutants of *Chlamydomonas reinhardtii* by fluorescence video imaging. Photosynth Res 61: 43–51

Küpper H, Šetlík I, Trtílek M and Nedbal L (2000) A microscope for two-dimensional measurements of in vivo chlorophyll fluorescence kinetics using pulsed measuring light, continuous actinic light and saturating flashes. Photosynthetica 38: 553–570

Lang M, Lichtenthaler H, M S, F H and JA M (1996) Fluorescence imaging of water and temperature stress in plant leaves. Plant Physiol 148: 613–621

Langsdorf G, Buschmann C, Sowinska M, Babani F, Mokry M, Timmermann F and Lichtenthaler H (2000) Multicolour fluorescence imaging of sugar beet leaves with different nitrogen status by flash lamp UV-excitation. Photosynthetica 38: 539–551

Lazár D (1999) Chlorophyll *a* fluorescence induction. Biochim Biophys Acta 1412: 1–28

Lichtenthaler HK and Babani F (2000) Detection of photosynthetic activity and water stress by imaging the red chlorophyll fluorescence. Plant Physiol Biochem 38: 889–895

Lichtenthaler H and Miche J (1997) Fluorescence imaging as a diagnostic tool for plant stress. Trends Plant Sci 2: 316–320

Lichtenthaler H, Lang M, Sowinska M, Heisel F and Miehe J (1996) Detection of vegetation stress via a new high resolution fluorescence imaging system. J Plant Physiol 148: 599–612

Lichtenthaler H, Lang M, Sowinska M, Summ P, Heisel F and Miehe J (1997) Uptake of the herbicide diuron as visualised by the fluorescence imaging technique. Botanica Acta 110: 158–163

Lichtenthaler H, Babani F, Langsdorf G and Buschmann C (2000) Measurement of differences in red chlorophyll fluorescence and photosynthetic activity between sun and shade leaves by fluorescence imaging. Photosynthetica 38: 521–529

Lohaus G, Heldt H and Osmond C (2000) Infection with phloem limited Abutilon Mosaic Virus causes localized carbohydrate accumulation in leaves of *Abutilon striatum*: Relationships to symptom development and effects on chlorophyll fluorescence quenching during photosynthetic induction. Plant Biol. 2: 161–167

Lootens P and Vandecasteele P (2000) A cheap chlorophyll *a* fluorescence imaging system. Photosynthetica: 53–56

Mazza A, Boccalandro H, CV G, Battista D, Scopel D and Ballare C (2000) Functional significance and induction by solar radiation of ultra-violet absorbing sunscreens in field-grown soybean crops. Plant Physiol. 122: 117–125

Mehta M, Sarafis V and Critchley C (1999) Thylakoid membrane architecture. Plant Physiol 26: 709–716

Meyer S and Genty B (1998) Mapping intercellular CO_2 mole fraction (C_I) in *Rosa rubiginosa* leaves fed with abscisic-acid

by using chlorophyll fluorescence imaging — significance of C_I estimated from leaf gas-exchange. Plant Physiol 116: 947–957

Meyer S and Genty B (1999) Heterogeneous inhibition of photosynthesis over the leaf surface of *Rosa rubiginosa* L. during water stress and abscisic acid treatment: Induction of a metabolic component by limitation of CO_2 diffusion. Planta 210: 126–131

Miles C and Daniel D (1973) A rapid screening technique for photosynthetic mutants of higher plants. Plant Sci Lett 1: 237–240

Mott K, Cardon Z and JA B (1993) Asymmetric patchy stomatal closure for the two surfaces of *Xanthium strumarium* L. leaves at low humidity. Plant Cell Environ 16: 25–34

Moya I, Camenen L, Latouche G, Mauxion C, Evain S and Cerovic Z (1998) An instrument for the measurement of sunlight excited plant fluorescence. In: Garab G (ed) Photosynthesis: Mechanisms and Effects, pp 4265–4270. Kluwer Academic Publishers, Dordrecht

Nedbal L and Březina V (2002) Complex metabolic oscillations in plants forced by harmonic irradiance. Biophys J 83: 2180–2189

Nedbal L and Koblížek M (2004) Chlorophyll fluorescence as a reporter on in vivo electron transport and regulation in plants. In: Grimm B, Porra R, Rüdiger W and Scheer H (eds) Biochemistry and Biophysics of Chlorophylls. Kluwer Academic Press, Dordrecht, in press

Nedbal L, Trtílek M and Kaftan D (1999) Flash fluorescence induction: A novel method to study regulation of Photosystem II. J Photochem Photobiol B 48: 154–157

Nedbal L, Soukupová J, Kaftan D, Whitmarsh J and Trtílek M (2000a) Kinetic imaging of chlorophyll fluorescence using modulated light. Photosynth Res 66: 3–12

Nedbal L, Soukupová J, Whitmarsh J and Trtílek M (2000b) Postharvest imaging of chlorophyll fluorescence from lemons can be used to predict fruit quality. Photosynthetica 38: 571–579

Ning L, Edwards G, Strobel G, Daley L and Callis J (1995) Imaging fluorometer to detect pathological and physiological change in plants. Appl Spectroscopy 49: 1381–1389

Ning L, Petersen B, Edwards G, Daley L and Callis J (1997) Recovery of digital information stored in living plant leaf photosynthetic apparatus as fluorescence signals. Appl Spectroscopy 51: 1–9

Niyogi K, Björkman O and Grossman A (1997) *Chlamydomonas* xanthophyll cycle mutants identified by video imaging of chlorophyll fluorescence quenching. Plant Cell 9: 1369–1380

Niyogi K, Grossman A and Björkman O (1998) *Arabidopsis* mutants define central role for the xanthophyll cycle in the regulation of photosynthetic energy conversion. Plant Cell 10: 1121–1134

Omasa K, Shimazaki K, Aiga I, Laracher W and Onoe M (1987) Image analysis of chlorophyll fluorescence transients for diagnosing the photosynthetic system of attached leaves. Plant Physiol 84: 748–752

Osmond B, Schwartz O and Gunning B (1999a) Photoinhibitory printing on leaves, visualised by chlorophyll fluorescence imaging and confocal microscopy, is due to diminished fluorescence from grana. Aust J Plant Physiol 26: 717–724 **[Are Osmond B and Osmond C the same person? If not this should not be 1999a and the other ref below should not be 1999b. Please check.]**

Osmond C, Berry J, Balachandran S, Büchen-Osmond C, Daley P and Hodgson R (1990) Potential consequences of virus infection for shade-sun acclimation of leaves. Botanica Acta 103: 226–229

Osmond C, Daley P, Badger M and Luttge U (1998) Chlorophyll fluorescence quenching during photosynthetic induction in leaves of *Abutilon striatum* Dicks. infected with Abutilon mosaic virus, observed with a field-portable imaging system. Botanica Acta 111: 390–397

Osmond C, Kramer D and Luttge U (1999b) Reversible, water stress-induced non-uniform chlorophyll fluorescence quenching in wilting leaves of *Potentilla reptans* may not be due to patchy stomatal responses. Plant Biol. 1: 618–624

Oxborough K and Baker N (1997a) Resolving chlorophyll-*a* fluorescence images of photosynthetic efficiency into photochemical and nonphotochemical components—calculation of qp and Fv′/Fm′ without measuring Fo′. Photosynth Res 54: 135–142

Oxborough K and Baker R (1997b) An instrument capable of imaging chlorophyll-*a* fluorescence from intact leaves at very-low irradiance and at cellular and subcellular levels of organization. Plant Cell Environ 20: 1473–1483

Peterson R and Aylor D (1995) Chlorophyll fluorescence induction in leaves of *Phaseolus vulgaris* infected with bean rust (*Uromyces appendiculatus*). Plant Physiol 108: 163–171

Peterson R and Havir E (2000) A nonphotochemical-quenching-deficient mutant of *Arabidopsis thaliana* possessing normal pigment composition and xanthophyll-cycle activity. Planta 210: 205–214

Rascher U, Hütt M-T, Siebke K, Osmond B, Beck F and Lüttge U (2001) Spatiotemporal variation of metabolism in a plant circadian rhythm: The biological clock as an assembly of coupled individual oscillators. Proc Natl Acad Sci USA 98: 11801–11805

Rolfe S and Scholes J (1995) Quantitative imaging of chlorophyll fluorescence. New Phytologist 131: 69–79

Scholes J and Rolfe S (1996) Photosynthesis in localised regions of oat leaves infected with crown rust (*Puccinia coronata*): Quantitative imaging of chlorophyll fluorescence. Planta 199: 573–582

Schreiber U, Schliwa U and Bilger W (1986) Continuous recording of photochemical and non-photochemical chlorophyll fluorescence quenching with a new type of modulation fluorometer. Photosynth Res 10: 51–62

Shikanai T, Shimizu K, Endo T and Hashimoto T (1998) Screening of *Arabidopsis* mutants lacking downregulation of Photosystem II using an imaging system of chlorophyll fluorescence. In: Garab G, Photosynthesis: Mechanisms and Effects, pp 4293–4296. Kluwer Academic Publishers, Dordrecht

Siebke K and Weis E (1995a) Assimilation images of leaves of *Glechoma hederacea*: Analysis of non-synchronous stomata related oscillations. Planta 196: 155–165

Siebke K and Weis E (1995b) Imaging of chlorophyll-a fluorescence in leaves—topography of photosynthetic oscillations in leaves of *Glechoma hederacea*. Photosynth Res 45: 225–237

Simon-Blecher N, Achituv Y and Malik Z (1996) Effect of epibionts on the microdistribution of chlorophyll in corals and its detection by fluorescence spectral imaging. Marine Biol 126: 454–763

Soukupová J, Smatanová S, Nedbal L and Jegorov A (2003) Plant

response to destruxins visualized by imaging of chlorophyll fluorescence. Physiol Plantarum 118: 1–8

Strasser RJ, Srivastava A and Tsimilli-Michael M (1998) The fluorescence transient as a tool to characterize and screen photosynthetic samples. In: Yunus M, Pathre U and Mohanty P (eds) Probing Photosynthesis: Mechanism, Regulation and Adaptation, pp 1–53. Taylor and Francis, London

Takahashi K, Mineuchi K, Nakamura T, Koizumi M and Kano H (1994) A system for imaging transverse distribution of scattered light and chlorophyll fluorescence in intact rice leaves. Plant Cell Environ 17: 105–110

Tyystjärvi E, Koski A, Keranen M and Nevalainen O (1999) The Kautsky curve is a built-in barcode. Biophys J 77: 1159–1167

Vácha F, Vácha M, Bumba L, Hashizume K and Tani T (2000) Inner structure of intact chloroplasts observed by a low temperature laser scanning microscope. Photosynthetica 38: 493–496

Varotto C, Pesaresi P, Maiwald D, Kurth J, Salamini F and Leister D (2000) Identification of photosynthetic mutants of *Arabidopsis* by automatic screening for altered effective quantum yield of Photosystem 2. Photosynthetica 38: 497–504

Velthuys B (1981) Electron dependent competition between plastoquinone and inhibitors for binding to Photosystem II. FEBS Lett 126: 277–281

Vogelmann T, Nishio J and Smith W (1996) Leaves and light capture — light-propagation and gradients of carbon fixation within leaves. Trends Plant Sci 1: 65–70

Weis E, Meng Q, Siebke K, Lippert K and Esfeld P (1998) Topography of leaf carbon metabolism as analyzed by chlorophyll-*a* fluorescence. In: Garab G (ed) Photosynthesis: Mechanisms and Effects, pp 4259–4264. Kluwer Academic Publishers, Dordrecht

Yanase D and Andoh A (1992) Translocation of photosynthesis — inhibiting herbicides in wheat leaves measured by phytofluorography, the chlorophyll fluorescence imaging. Pesticide Biochem Physiol 44: 60–67

Zangerl AR, Hamilton JG, Miller TJ, Crofts AR, Oxborough K, Berenbaum MR and DeLucia EH (2002) Impact of folivory on photosynthesis is greater than the sum of its holes. Proc Natl Acad Sci USA 99: 1088-1091